Bearing Defect and Misalignment Diagnostics Using Local Regularity and Sparse Frequency Analysis

Juhani Nissilä[1] Jouni Laurila[1] Keijo Ruotsalainen[2] Toni Liedes[1]

[1]Intelligent Machines and Systems, University of Oulu, PO Box 4200, 90014 Oulu, Finland,
{juhani.nissila,jouni.laurila,toni.liedes}@oulu.fi
[2]Applied and Computational Mathematics, University of Oulu, PO Box 4500, 90014 Oulu, Finland,
keijo.ruotsalainen@oulu.fi

Abstract

A local regularity signal can be estimated from a vibration measurement with the help of the continuous wavelet transform (CWT). The resulting local regularity signal contains a lot of diagnostic information about different faults states of a machine. It is also typically a sparse signal and thus not well suited for frequency analysis using the discrete Fourier transform (DFT). In this paper, the frequency analysis of the local regularity signal is performed using the Lomb-Scargle periodogram. Another possibility is to use the methods of compressed sensing. Vibration measurements from different fault states from test rigs are utilized in validating the proposed method and comparing it with other methods. The induced fault conditions include a bearing inner ring defect and misalignment of a claw clutch. The results are compared to more traditional spectra calculated directly from the vibration measurement, such as the spectrum of the squared envelope.

Keywords: Hölder regularity, continuous wavelet transform, sparse signals, Lomb-Scargle periodogram, compressed sensing, envelope analysis

1 Introduction

When the CWT of a signal is calculated using a real-valued wavelet, its absolute values form continuous ridges which converge towards the smaller scales. These modulus maxima ridges of the estimated CWT reveal the locations of irregularities in the signal and from their rate of decay, pointwise Hölder exponents of the irregularities can also be read (Mallat and Hwang, 1992). If we don't consider fractal signals, then there are typically only a finite amount of irregularities in a signal and thus only a finite amount of modulus maxima ridges in the CWT. The resulting local regularity signal, i.e. a signal which shows the estimated Hölder regularities or constants related to the sizes of the ridges and their locations, is thus a sparse signal. When these local regularity signals are calculated from vibration measurements of machines, they may contain useful diagnostic information. They have been shown to be useful for diagnosing for example gear tooth cracks and completely lost gear teeth (Loutridis and Trochidis, 2004), local bearing defects (Kotila et al., 2010) and misalignment of a claw clutch and bearing lubrication problems (Nissilä and Laurila, 2019). In (Miao and Makis, 2007) a feature vector calculated from the wavelet modulus maxima ridges is fed to a hidden Markov model for fault classification. Multifractal features extracted from vibration signals are used in bearing diagnostics in (Du et al., 2014).

Wavelet-based methods for extracting weak transients from vibration signals have been successfully applied with bearing faults (Wang et al., 2015) and gear faults (Fan et al., 2015). Wavelet transform was also used for detecting angular misalignment in (Saari et al., 2015). There are also several studies where some kind of sparse representations in some basis are sought and these sparse decompositions also turn out to be useful for gear fault (Zhang et al., 2021; Li et al., 2018) and bearing fault diagnostics (Li et al., 2019; Chen et al., 2017; He et al., 2016).

In machine diagnostics of rotating or reciprocating machines, frequency analysis of measured vibration signals is typically utilized. Methods based on the DFT are easily available, since the measurements are typically equispaced in time. When equispaced measurements are not available, different methods for frequency analysis are needed. This is often the case in astronomical time series and for that reason Lomb and Scargle developed a method that is now called the Lomb-Scargle periodogram (Lomb, 1976; Scargle, 1982). In this study, we calculate these spectra from signals generated using local regularity analysis and they are compared to the spectra of the squared envelope calculated directly from the acceleration measurements. Envelope analysis is a benchmark method in machine diagnostics for diagnosing bearing faults and other faults which cause cyclostationary vibration signatures (Randall et al., 2001).

2 Materials and methods

2.1 Measurements

In this paper, two fault states with six different levels of severity are used for comparing the proposed signal processing methods. The first fault state is a local inner ring fault in a roller bearing. The test rig manufactured by SPM Instrument is shown in Figure 1. The three bearings at the

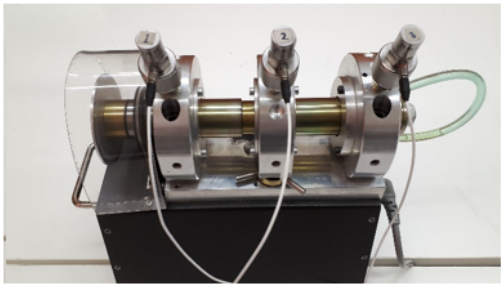

Figure 1. The bearing test rig.

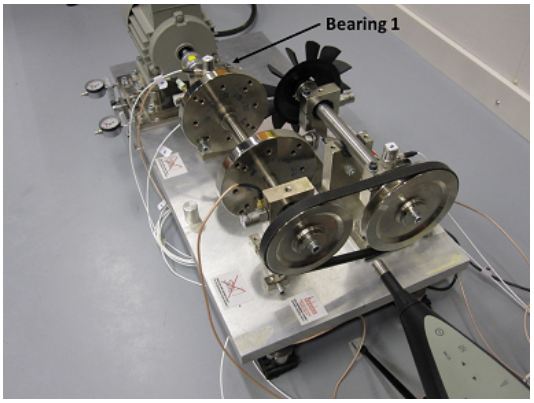

Figure 2. The misalignment test rig.

top support the axle that is driven by a chain drive. The inner ring fault is located in the middle bearing and it is a simple groove that is cut into the inner race. The middle bearing housing can be tightened using a screw and this method gives the six different levels of load. The measurements that we use are recorded using the accelerometer 2 seen in Figure 1 and it is mounted to the bearing housing using a magnet. Sampling frequency is 25.6 kHz and 10 s long measurements from each load level are used.

The test rig used for misalignment measurements is shown in Figure 2. Coupling misalignment in the horizontal direction was induced by moving the motor while keeping the vertical and angular alignment constant. Horizontal measurements from bearing 1 are utilized in this study and the accelerometer was screwed directly into the bearing housing. Sampling frequency is 50 kHz and signal length is 15 s for each misalignment state. The test rig is presented in more detail in (Lahdelma and Laurila, 2012; Lahdelma et al., 2011).

In both measurements, the accelerometer type was Wilcoxon Research 726 with a linear (±5 %) frequency range from 2 Hz to 10 kHz.

2.2 Signal processing

The spectrum of the discrete signal $\boldsymbol{x} = (x_0, \ldots, x_{N-1})^{\mathsf{T}}$ of length $T = \Delta t \cdot N$ is defined using the *discrete Fourier transform* (DFT)

$$\mathscr{F}\{\boldsymbol{x}\}_k = X_k = \frac{1}{N}\sum_{n=0}^{N-1} x_n e^{-i2\pi kn/N}, \tag{1}$$

and the *inverse transform* (IDFT) returns the signal at the sample points (Briggs and Henson, 1995)

$$\mathscr{F}^{-1}\{\boldsymbol{X}\}_n = x_n = \sum_{k=0}^{N-1} X_k e^{i2\pi kn/N}. \tag{2}$$

The *cyclic convolution* of two sampled signals is

$$(\boldsymbol{x} * \boldsymbol{y})_n = \sum_{l=0}^{N-1} x_l\, y_{n-l}, \tag{3}$$

and its DFT is (Briggs and Henson, 1995)

$$\mathscr{F}\{(\boldsymbol{x} * \boldsymbol{y})\}_k = N X_k Y_k. \tag{4}$$

For a discrete time random signal $\mathbf{X}_n$, we define the *squared envelope* (SE) with the expected values $\mathrm{E}\left[|\mathbf{X}_n|^2\right]$ and the *squared envelope spectrum* (SES) by

$$\mathrm{SES}\{\mathbf{X}_n\}(f_c) = \lim_{M\to\infty} \frac{1}{2M+1} \sum_{n=-M}^{M} \mathrm{E}\left[|\mathbf{X}_n|^2\right] e^{-i2\pi f_c n}. \tag{5}$$

In (Dandawate and Giannakis, 1995) it has been proved that under some assumptions, a simple DFT of the squared samples

$$\mathrm{SES}\{\mathbf{X}_n\}\left(\frac{k}{N}\right) \approx \frac{1}{N}\sum_{n=0}^{N-1} \left|x_n\right|^2 e^{-i2\pi kn/N} \tag{6}$$

converges in the mean-square sense to the SES at the cyclic frequency $f_c = k/N$ as $N \to \infty$.

Let us define informally, that a *wavelet* is a brief oscillation. We denote the wavelet by ψ and we want to dilate it by $s > 0$ but retain its L^1 norm

$$\psi_s(t) = \frac{1}{s}\psi\left(\frac{t}{s}\right). \tag{7}$$

The *continuous wavelet transform* (CWT) of a continuous time signal x is

$$\begin{aligned} Wx(s,t) &= (x * \psi_s)(t) \\ &= \frac{1}{s}\int_{-\infty}^{\infty} x(\tau)\psi\left(\frac{t-\tau}{s}\right) \mathrm{d}\tau. \end{aligned} \tag{8}$$

Here t is the point of interest in the signal and s is the positive *scale* that tells how much the wavelet is dilated.

The wavelet that we have chosen for this study is the second derivative of a *central B-spline* (Unser and Blu, 2000) and its DFT is

$$\begin{aligned} B_k &= \frac{1.83}{N}\left(\frac{i2\pi k}{N}\right)^2 \left|\frac{\sin(2\pi k/N)}{2\pi k/N}\right|^5, \\ B_{N/2} &= \frac{1.83}{N}\pi^2\cos(\pi)\left|\frac{\sin(\pi)}{\pi}\right|^5 = 0, \end{aligned} \tag{9}$$

where $-N/2 < k < N/2$. The negative frequencies correspond to $N/2 < k < N$ in our definition of the DFT.

The constant is chosen so that the wavelet's l^1 norm $\|\mathscr{F}^{-1}\{\boldsymbol{B}\}\|_1$ is roughly equal to 1.

The discrete estimate of the CWT at scale s is denoted by $W\boldsymbol{x}_{s,n}$. To calculate its DFT, we first window the measured signal $\boldsymbol{x}$ with a smooth window function called the *Planck-taper window* $\boldsymbol{w}$ (McKechan et al., 2010), i.e. compute $x_n w_n$, calculate its DFT $\mathscr{F}\{x_n w_n\}_k$ and then estimate the DFT of the wavelet transform using (4)

$$\mathscr{F}\{W\boldsymbol{x}_{s,n}\}_k = N\mathscr{F}\{x_n w_n\}_k B_{sk}. \tag{10}$$

Finally, we obtain $W\boldsymbol{x}_{s,n}$ at the desired scales using the IDFT.

Let $\mu \geq 0$. A function x is *pointwise μ-Hölder continuous* at t_0 if

$$|x(t_0+h) - P_m(h)| \leq C|h|^{\mu}, \tag{11}$$

for small values of $|h|$ and P_m is a polynomial of degree $m \leq \mu$.

When traversing a CWT through the scales, a series of connected local maxima or minima are often observed (Mallat, 2009). These are *wavelet transform modulus maxima ridges* (WTMM ridges). In (Mallat and Hwang, 1992), it has been proved that if there are no such ridges at the fine scales on some interval, then x is uniformly Hölder continuous on that interval. Conversely, they proved under some assumptions that if there exists a constant C and a scale s_0 such that all the modulus maxima of $Wx(s,t)$ belong to the cone

$$|t - t_0| < Cs, \tag{12}$$

then x is μ-Hölder at t_0 if and only if

$$|Wx(s,t)| \leq As^{\mu}, \tag{13}$$

at each modulus maxima inside the cone (12). This result means, that if one can recognize the WTMM ridges of isolated irregularities, then their Hölder exponents can be estimated using logarithms and a least squares line fit to

$$\log(|Wx(s,t)|) \leq \log(A) + \mu\log(s). \tag{14}$$

The constant A is related to the height of the ridge, and will also be useful.

The *Lomb-Scargle periodogram* estimates the *power spectral density* (PSD) at the frequencies f of the signal $\boldsymbol{x}$ which has been nonuniformly sampled at the points t_n

$$\begin{aligned} \mathrm{P_{LS}}\{\boldsymbol{x}\}(f) = &\frac{\left(\sum_n x_n \cos\left(2\pi f(t_n-\tau)\right)\right)^2}{2\sum_n \cos^2\left(2\pi f(t_n-\tau)\right)} \\ &+ \frac{\left(\sum_n x_n \sin\left(2\pi f(t_n-\tau)\right)\right)^2}{2\sum_n \sin^2\left(2\pi f(t_n-\tau)\right)}, \end{aligned} \tag{15}$$

where the delay τ is chosen for each frequency f by

$$\tau = \frac{1}{4\pi f}\tan^{-1}\left(\frac{\sum_n \sin(4\pi f t_n)}{\sum_n \cos(4\pi f t_n)}\right). \tag{16}$$

The *discrete cosine transform* (DCT) according to (Ahmed et al., 1974) is defined by

$$\begin{aligned} \mathrm{DCT}\{\boldsymbol{x}\}_0 &= \frac{\sqrt{2}}{N}\sum_{n=0}^{N-1} x_n, \\ \mathrm{DCT}\{\boldsymbol{x}\}_k &= \frac{2}{N}\sum_{n=0}^{N-1} x_n \cos\frac{(2n+1)k\pi}{2N}, \quad k = 1,...,N-1. \end{aligned} \tag{17}$$

When searching for a sparse representation of a discrete signal $\boldsymbol{x} = (x_0,\ldots,x_{N-1})^{\mathsf{T}}$ in some basis, the following minimization problem is addressed

$$\min\|\boldsymbol{v}\|_0, \qquad \text{such that} \qquad \|\boldsymbol{x} - \Theta\boldsymbol{v}\|_2 < \varepsilon. \tag{18}$$

The l^0 pseudo-norm is simply the number of nonzero components of the vector. Many solution algorithms replace it with the l^1 norm. In this paper, the vector $\boldsymbol{v}$ is the sparse DCT of $\boldsymbol{x}$ and the matrix Θ represents the inverse transform and the restriction to using only the sparse signal measurement points. Only those rows which correspond to the sparse local regularity signal are nonzero. To make the problem more tractable, we also limit our attention to only a small portion of the DCT spectrum, and thus only columns of Θ up to some desired maximum frequency are included. The sparse solution in the DCT spectrum is searched using the *orthogonal matching pursuit* (OMP) algorithm (Pati et al., 1993; Mallat, 2009). The DCT is favored in this sparse approximation problem instead of the DFT because it only has one coefficient for each frequency, i.e. no negative frequencies.

3 Results and discussion

3.1 Acceleration measurements and their squared envelope spectra, bearing fault

Calculations were performed with MATLAB R2020b. Samples from the acceleration measurements of the six different load levels in the bearing test are shown in Figure 3. Case 0 is the smallest load level and Case 5 is the largest. It is important to notice, that the shocks caused by the fault are lowest in Case 1 and then start to increase again when the load level is further increased. The rotational frequency of the shaft is roughly 18.6 - 18.2 Hz depending on the load level. As this is also the rotational frequency of the faulty bearing inner race, the shocks caused by the fault are amplified once per revolution of the axle, i.e. whenever the fault passes the loading region. When the fault is passing the loading region, several shocks between the fault and rollers occur and these become more visible when the load level increases. The frequency of these shocks (*ballpass frequency, inner ring*, or BPFI) is roughly 140 - 147 Hz depending on the rotational frequency of the shaft.

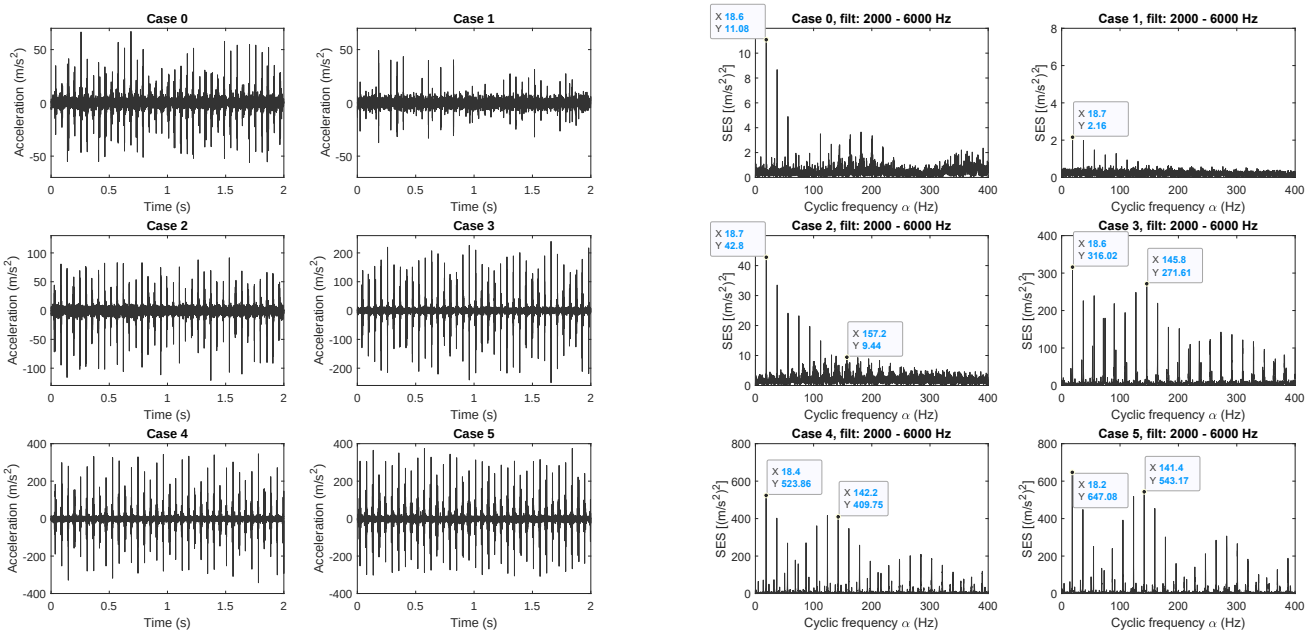

Figure 3. Acceleration measurements from the bearing test rig and their squared envelope spectra.

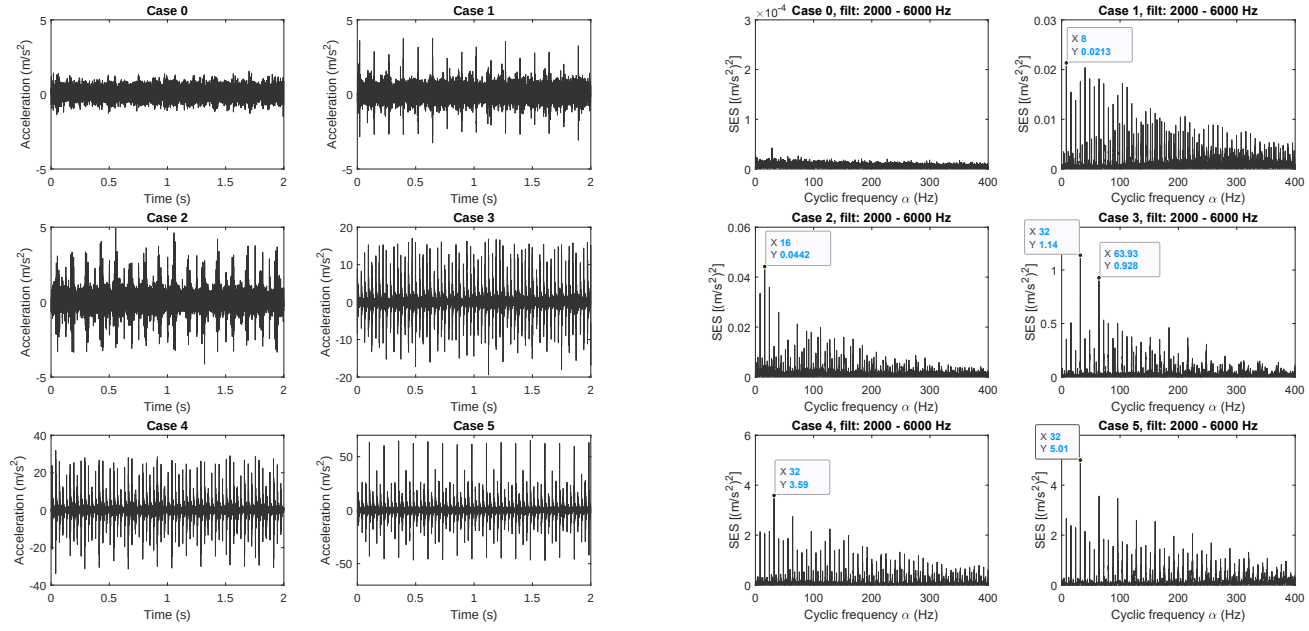

Figure 4. Acceleration measurements from the misalignment test rig and their squared envelope spectra.

DOI: 10.3384/ecp21185171

The SES of these load cases in Figure 3 are calculated from 10 s long signals and they show us that the strong amplitude modulation is visible as peaks at the shaft speed and its multiples in all load cases. From Case 3 onwards, the BPFI and its sidebands spaced shaft speed apart become clearly visible as a distinct pattern, although faint signs of this pattern already exist in Cases 0 and 2.

3.2 Acceleration measurements and their squared envelope spectra, misalignment

Samples from the acceleration measurements of the six different misalignment states are shown in Figure 4. Case 0 is the no misalignment state and in the following cases the misalignment increases in 0.1 mm increments. Shaft speed is roughly 8 Hz and it is clear, that in Case 1 and 2 there are shocks which repeat mainly at this frequency. From Case 3 onwards, the shocks become more pronounced and they repeat 4 times in every revolution of the shaft, i.e. at the frequency 32 Hz. In Case 5 it is also noticeable that the 4 impacts per revolution are unique and they repeat in a similar fashion. Especially one of them is much bigger in amplitude than the others. The claw clutch located between the motor and bearing 1 has a 4-tooth flexible element which explains these phenomena.

The SES of the different misalignment cases calculated from 15 s long signals are also shown in Figure 4. Shaft speed (8 Hz) and its multiples dominate the spectra from Case 1 onwards. From Case 3 onwards, 32 Hz and its multiples have the largest amplitudes. In these cases, it is also possible to interpret the other multiples of 8 Hz as sidebands of 32 Hz and its multiples. This matches our observations from the time domain signals, mainly that the shocks which occur at 1/32 s intervals are also amplitude modulated by the shaft speed especially in Case 5.

3.3 Local regularity signals and their L-S periodograms and DCT spectra, bearing fault

The CWT of the bearing measurements are estimated at the scales $s = 1.5, 1.6, \ldots, 5.9, 6$, their WTMM ridges are detected and irregularities whose constants A are above 1 are saved. The Hölder exponents and constants A from the bearing measurements are shown in Figure 5. Also here we can see that the vibration is smoothest in Case 1. The Hölder exponents reach quite large negative values. Even in Cases 0 and 1 there are a couple of irregularities with exponents that are less than -3. Such large negative values were also observed in (Nissilä and Laurila, 2019; Kotila et al., 2010) in cases of dry bearing and local bearing faults. We also observe that the amount of irregularities increases with the load level and their constants A get bigger.

For frequency analysis, it was observed that the constants A are more suitable than the Hölder exponents. Figure 6 shows the L-S periodograms of the constants A from all of the load cases. In Case 1 the only recognizable frequency is the axle speed. In Case 0 its multiples are visible and also BPFI with a couple of sidebands spaced axle speed apart. This structure is more emphasized in Case 2 and from Case 3 onwards the axle speed has the biggest amplitude followed with the BPFI. There are also numerous sidebands spaced axle speed apart around BPFI and its multiple. The load level is quite easy to read of from the increasing amplitudes and when compared to the SE spectra in Figure 3, the BPFI is more easily recognized in Cases 0 and 2.

The DCT spectra of constants A in Figure 6 are searched using sparse solutions with 60, 30, 100, 100, 100 and 100 components for the Cases 0 to 5 and for the frequencies shown. In these spectra, we can also observe the BPFI in Cases 0 and 2 and it becomes more distinctive in Cases 3, 4, and 5. The increase in the amplitude of the BPFI with fault severity is not as big as in the L-S spectra.

3.4 Local regularity signals and their L-S periodograms and DCT spectra, misalignment

The CWT of the misalignment measurements are estimated at the scales $s = 1.5, 1.6, \ldots, 5.9, 6$, their WTMM ridges are detected and irregularities whose constants A are above 0.05 are saved. The Hölder exponents and constants A from the misalignment measurements are shown in Figure 7. The Hölder exponents are mainly positive and we see that the number of irregularities and also their constants A increase with the severity of the fault. The amplitudes of the constants A also seem to reflect the periodicity of the shocks caused by the fault.

Also for this fault state, the constants A were better suited for sparse frequency analysis than the Hölder exponents. Figure 8 shows the L-S periodograms of the constants A from all of the fault cases. The amount of irregularities was so small in Case 0, that the estimated spectrum is almost white noise. In Case 1 there are many multiples of the shaft speed (8 Hz) and 8 times the shaft speed has the biggest amplitude. In Case 2 we see that 2 and 11 times the shaft speed are the largest. From Case 3 onwards, four times the shaft speed (32 Hz) is the dominant frequency and it has significant multiples. They also have small sidebands mainly 8 Hz apart. The frequency contents of these spectra are very similar to the SE spectra in Figure 4. The main difference is that the frequency 32 Hz and its multiples are much more prevalent from Case 3 onwards. We can thus confirm, that the diagnostic capability is roughly the same compared to the SES, but possibly the specific nature of the 4-tooth elastic spider element becomes more pronounced when using the L-S spectra of constants A.

The DCT spectra of constants A in Figure 8 are searched using 10, 30, 200, 200, 200 and 200-sparse solutions for the Cases 0 to 5 and for the frequencies shown. It was necessary to decrease the sparsity to obtain spectra where the fault frequency 32 Hz and its multiples become most dominant. When compared to the L-S spectra, it is again observed that the increase in the amplitude of the fault frequency between the cases is not as big. Fault frequency multiples also tend to increase with the severity of the fault, but there is some variation. In Case 1, the frequency 64 Hz has the biggest amplitude.

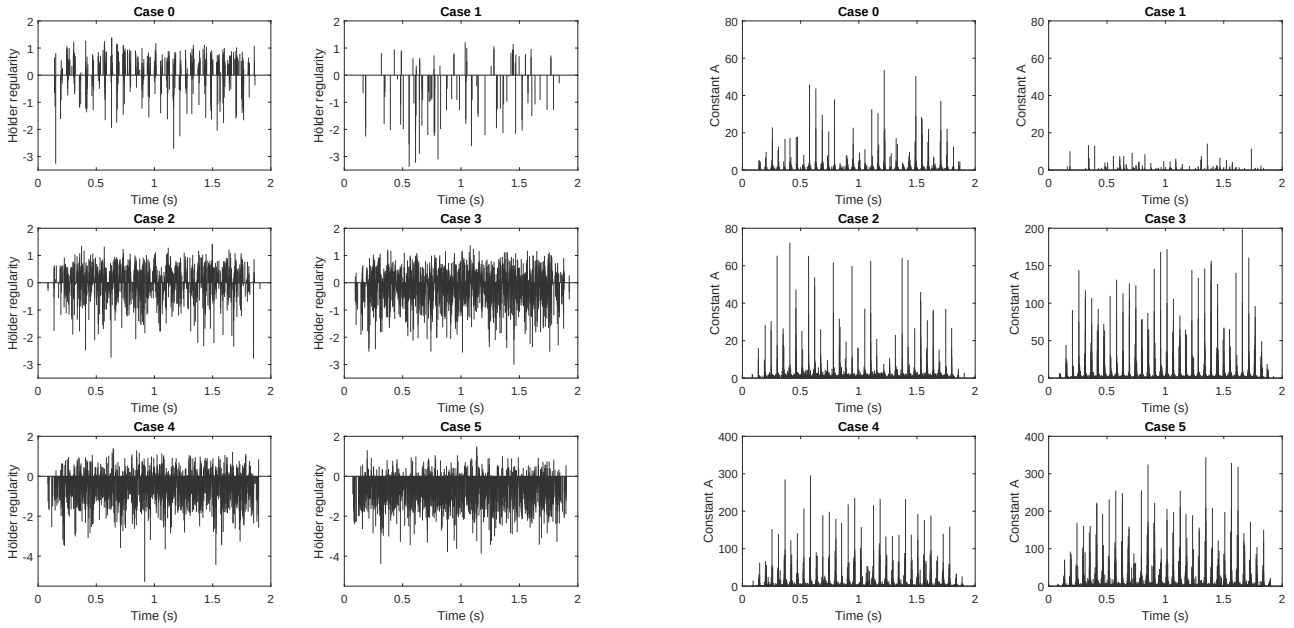

Figure 5. Hölder exponents and constants *A* of the local irregularities from the bearing test rig acceleration measurements.

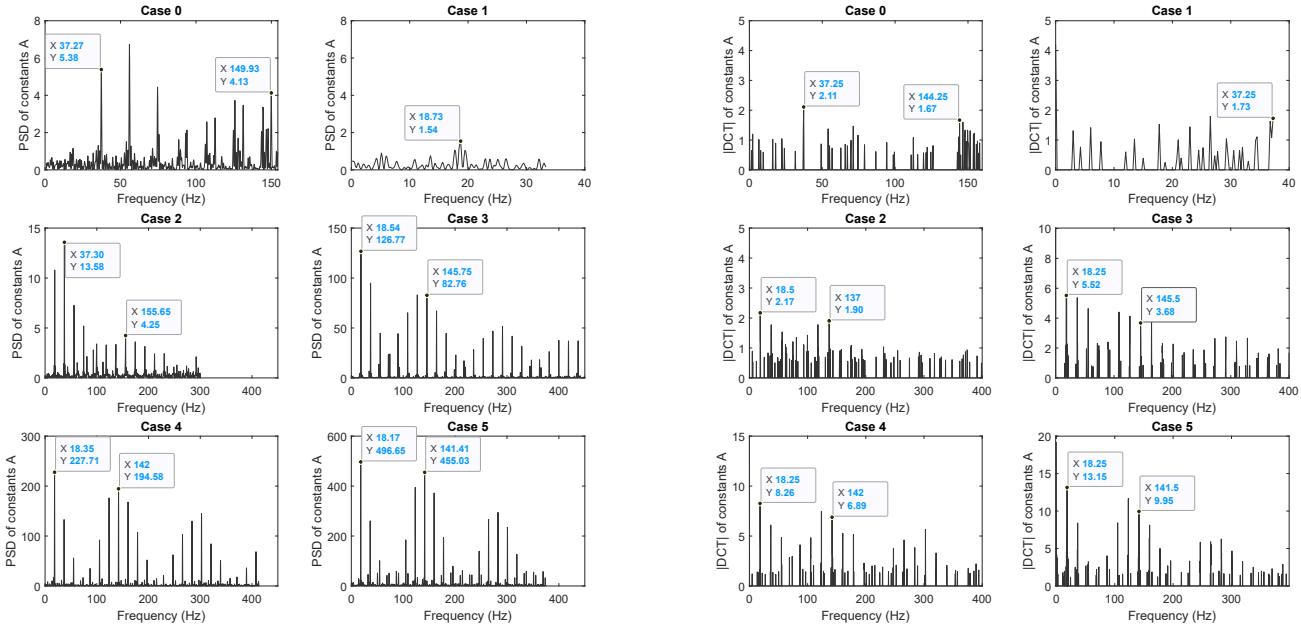

Figure 6. Lomb-Scargle periodograms and absolute values of discrete cosine transforms of the constants *A* from the bearing test rig acceleration measurements.

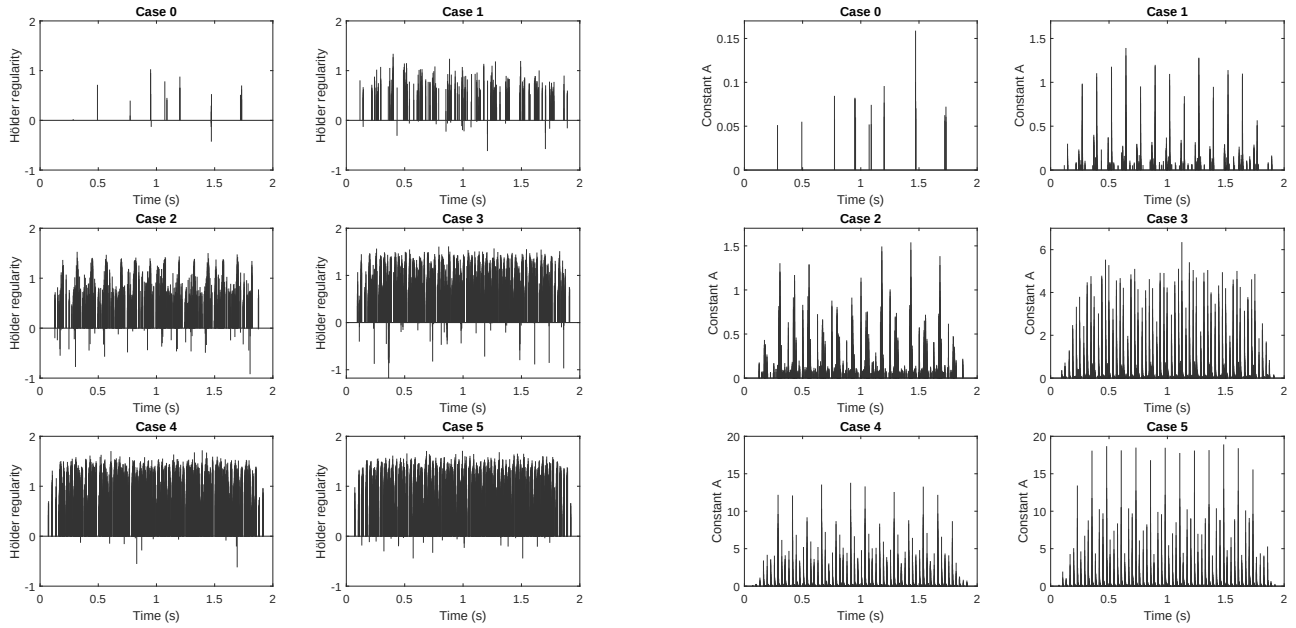

Figure 7. Hölder exponents and constants A of the local irregularities from the misalignment test rig acceleration measurements.

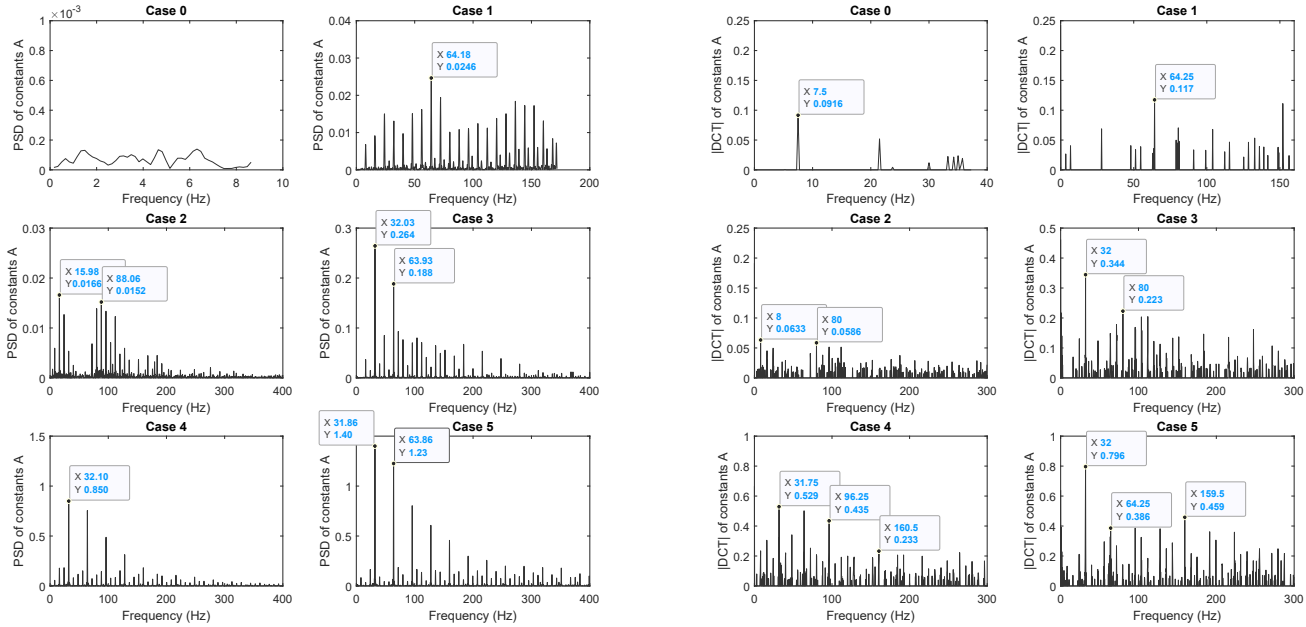

Figure 8. Lomb-Scargle periodograms and absolute values of discrete cosine transforms of the constants *A* from the misalignment test rig acceleration measurements

4 Conclusions

Local regularity analysis in the context of vibration monitoring has been studied for a couple of decades, but mainly as a tool in time domain analysis. The spectral analysis of local irregularities is not a simple task because of their sparse nature. However, the spectra of the constants A of the local irregularities carries at least as much diagnostic information as the squared envelope spectra calculated directly from acceleration signals. All of the tested methods contain different tunable parameters. For SES, these are mainly the bandpass filter's lower and upper limits. For the local regularity analysis, they are the choice of wavelet, the computed scales and the lower limit on how small constants A are taken into the analysis. The computation of the L-S spectrum of constants A is quite straightforward, but when its sparse DCT spectrum is estimated instead, the optimization algorithm and its parameters become tunable parameters as well. Because these parameters are so different for these methods, it is not easy to compare them fairly

For the examples in this paper, 10 and 15 s long signals were used for the estimation of the SES and only 2 s long signals were used for the local regularity analysis. Because of the result (6), it is advantageous to use long signals to estimate the SES. The calculation of the SES is also so simple, that the computational cost is still quite low. In contrast, it is computationally more costly to calculate the local regularity estimation and its sparse spectral analysis for long signals. But we have also demonstrated, that even only 2 s long signals are long enough for good frequency analysis results for both of the examples in this paper.

It is easy to set the lower limit on the constants A to such a level, that in the healthy condition the amount of irregularities is negligible and the spectrum is mostly white noise. This means that changes in the load or health of the machine become easily distinguishable. Especially the Lomb-Scargle periodograms of constants A were found to be very good at detecting and highlighting the fault frequencies.

References

N. Ahmed, T. Natarajan, and K. R. Rao. Discrete Cosine Transform. *IEEE Transactions on Computers*, C-23(1): 90–93, 1974. doi:10.1109/T-C.1974.223784.

W. Briggs and V. E. Henson. *The DFT: An Owner's Manual for the Discrete Fourier Transform*. Society for Industrial and Applied Mathematics, Philadelphia, PA, USA, 1995. ISBN 978-0-898713-42-8.

G. Chen, F. Liu, and W. Huang. Sparse discriminant manifold projections for bearing fault diagnosis. *Journal of Sound and Vibration*, 399: 330–344, 2017. doi:10.1016/j.jsv.2017.03.029.

A. V. Dandawate and G. B. Giannakis. Asymptotic theory of mixed time averages and kth-order cyclic-moment and cumulant statistics. *IEEE Transactions on Information Theory*, 41(1): 216–232, 1995. doi:10.1109/18.370106.

W. Du, J. Tao, Y. Li, and C. Liu. Wavelet leaders multifractal features based fault diagnosis of rotating mechanism. *Mechanical Systems and Signal Processing*, 43(1–2): 57–75, 2014. doi:10.1016/j.ymssp.2013.09.003.

W. Fan, G. Cai, Z. K. Zhu, C. Shen, W. Huang, and L. Shang. Sparse representation of transients in wavelet basis and its application in gearbox fault feature extraction. *Mechanical Systems and Signal Processing*, 56–57: 230–245, 2015. doi:10.1016/j.ymssp.2014.10.016.

W. He, Y. Ding, Y. Zi, and I. W. Selesnick. Sparsity-based algorithm for detecting faults in rotating machines. *Mechanical Systems and Signal Processing*, 72–73: 46–64, 2016. doi:10.1016/j.ymssp.2015.11.027.

V. Kotila, S. Lahdelma, and K. Ruotsalainen. Wavelet-Based Hölder Regularity Analysis in Condition Monitoring. In C. Constanda and M.E. Pérez, editors, *Integral Methods in Science and Engineering, Volume 2: Computational methods*, pages 233–242, Birkhauser, 2010. ISBN 978-0-8176-4896-1. doi:10.1007/978-0-8176-4897-8_22.

S. Lahdelma and J. Laurila. Detecting misalignment of a claw clutch using vibration measurements. In *Proceedings - 9th International Conference on Condition Monitoring and Machinery Failure Prevention Technologies, CM 2012 /MFPT 2012, June 2012, London, UK*, 2012. https://www.researchgate.net/publication/270048637_Detecting_Misalignment_of_a_Claw_Clutch_Using_Vibration_Measurements.

S. Lahdelma, J. Laurila, J. Strackeljan, and R. Hein. Separating Different Vibration Sources in Complex Fault Detection. In *Proceedings - 8th International Conference on Condition Monitoring and Machinery Failure Prevention Technologies, CM 2011 / MFPT 2011, June 2011, Cardiff, UK*, 2011. https://www.researchgate.net/publication/270048457_Separating_Different_Vibration_Sources_in_Complex_Fault_Detection.

G. Li, G. Tang, H. Wang, and Y. Wang. Blind source separation of composite bearing vibration signals with low-rank and sparse decomposition. *Measurement*, 145: 323–334, 2019. doi:10.1016/j.measurement.2019.05.099.

Y. Li, K. Ding, G. He, and X. Jiao. Non-stationary vibration feature extraction method based on sparse decomposition and order tracking for gearbox fault diagnosis. *Measurement*, 124: 453–469, 2018. doi:10.1016/j.measurement.2018.04.063.

N. R. Lomb. Least-squares frequency analysis of unequally spaced data. *Astrophysics and Space Science*, 39: 447–462, 1976. doi:10.1007/BF00648343.

S. Loutridis and A. Trochidis. Classification of gear faults using Hoelder exponents. *Mechanical Systems and Signal Processing*, 18(5): 1009–1030, 2004. doi:10.1016/j.ymssp.2004.01.007.

S. Mallat. *A Wavelet Tour of Signal Processing: The Sparse Way, Third Edition*. Academic Press, Burlington, MA, USA, 2009. ISBN 978-0-12-374370-1.

S. Mallat and W. L. Hwang. Singularity detection and processing with wavelets. *IEEE Transactions on Information Theory*, 38(2): 617–643, 1992. doi:10.1109/18.119727.

D. J. A. McKechan, C. Robinson, and B. S. Sathyaprakash. A tapering window for time-domain templates and simulated signals in the detection of gravitational waves from coalescing compact binaries. *Classical and Quantum Gravity*, 27: 084020. doi:10.1088/0264-9381/27/8/084020.

Q. Miao and V. Makis. Condition monitoring and classification of rotating machinery using wavelets and hidden Markov models. *Mechanical Systems and Signal Processing*, 21(2): 840–855, 2007. doi:10.1016/j.ymssp.2006.01.009.

J. Nissilä and J. Laurila. Diagnosing simultaneous faults using the local regularity of vibration signals. *Measurement Science and Technology*, 30: 045102, 2019. doi:10.1088/1361-6501/aaf8fa.

Y. C. Pati, R. Rezaiifar, and P.S. Krishnaprasad. Orthogonal matching pursuit: recursive function approximation with applications to wavelet decomposition. In *Proceedings - 27th Asilomar Conference on Signals, Systems and Computers, 1-3 November, 1993, Pacific Grove, CA, USA*, pages 40–44, 1993. doi:10.1109/ACSSC.1993.342465.

R. B. Randall, J. Antoni, and S. Chobsaard. The relationship between spectral correlation and envelope analysis in the diagnostics of bearing faults and other cyclostationary machine signals. *Mechanical Systems and Signal Processing*, 15(5): 945–962, 2001. doi:10.1006/mssp.2001.1415.

J. Saari, J. Odelius, J. Lundberg, and M. Rantatalo. Using wavelet transform analysis and the support vector machine to detect angular misalignment of a rubber coupling. In *Proceedings - Maintenance, Condition Monitoring and Diagnostics, Maintenance Performance Measurement and Management, MCMD 2015 / MPMM 2015, 30 September - 1 October, 2015 Oulu, Finland*, 2015. http://urn.kb.se/resolve?urn=urn:nbn:se:ltu:diva-66432.

J. D. Scargle. Studies in astronomical time series analysis. II. Statistical aspects of spectral analysis of unevenly spaced data. *Astrophysical Journal*, 263: 835–853, 1982. doi:10.1086/160554.

M. Unser and T. Blu. Fractional Splines and Wavelets. *SIAM Review*, 42(1): 43–67, 2000. doi:10.1137/S0036144598349435.

Y. Wang, G. Xu, L. Liang, and K. Jiang. Detection of weak transient signals based on wavelet packet transform and manifold learning for rolling element bearing fault diagnosis. *Mechanical Systems and Signal Processing*, 54–55: 259–276, 2015. doi:10.1016/j.ymssp.2014.09.002.

L. Zhang, Y. Li, L. Dong, X. Yang, X. Ding, Q. Zeng, L. Wang, and Y. Shao. Gearbox Fault Diagnosis Using Multiscale Sparse Frequency-Frequency Distributions. *IEEE Access*, 9: 113089–113099, 2021. doi:10.1109/ACCESS.2021.3104281.